PHYSICS AND CHEMISTRY OF SOLID STATE
V. 25, No. 3 (2024) pp. 605-616
Section: Physics

DOI: 10.15330/pcss.25.3.605-616

Vasyl Stefanyk Precarpathian National University

ФІЗИКА І ХІМІЯ ТВЕРДОГО ТІЛА
Т. 25, № 3 (2024) С. 605-616
Фізико-математичні науки

PACS: 82.70.-y, 82.33.Ln, 61.05.cp, 61.46.-w, 78.30.-j, 62.20.de, 75.75.-c

ISSN 1729-4428 (Print)
ISSN 2309-8589 (Online)

J. Mazurenko[1,2], L. Kaykan[3], V. Moklyak[3,4], M. Petryshyn[5], O. Mazurenko[5], S. Leleko[1]

Photocatalytic degradation of methylene blue in aqueous media using magnesium-substituted copper ferrite as a magnetic catalyst

[1]*Ivano-Frankivsk National Medical University, Ivano-Frankivsk, Ukraine, yumazurenko@ifnmu.edu.ua;*
[2]*Faculty of Physics and Applied Computer Science, AGH University of Krakow, Krakow, Poland, mazurenko@agh.edu.pl;*
[3]*G.V. Kurdyumov Institute for Metal Physics, N.A.S. of Ukraineб Kyov, Ukraine, larysa.kaykan@gmail.com;*
[4]*Ivano-Frankivsk National Technical University of Oil and Gas, Ivano-Frankivsk, Ukraine, volodymyr.mokliak@nung.edu.ua;*
[5]*Department of Computer Science, Vasyl Stefanyk Precarpathian National University, Ivano-Frankivsk, Ukraine, m.l.petryshyn@pnu.edu.ua*

In this study, copper nanosized ferrites substituted with magnesium ions were synthesized using the sol-gel self-combustion method, with polyethylene glycol (M_W=2000) serving as both fuel and chelating agent. Structural properties were investigated using X-ray diffraction. It was confirmed that all samples crystallized as cubic spinels with space group Fd3m. Optical studies showed band gaps increasing from 1.51 eV for $CuFe_2O_4$ to 1.62 eV for $MgFe_2O_4$, suggesting modifications in electronic structure due to magnesium substitution. Photocatalytic studies revealed that $CuFe_2O_4$ exhibited the most efficient degradation of Methylene Blue dye, with near-complete degradation at 160 minutes. Magnesium-substituted samples ($x = 0.4$ and $x = 0.6$) also showed significant degradation, though at a slower rate compared to pure $CuFe_2O_4$. Photocatalytic performance, particularly in degrading Methylene Blue, was evaluated using various kinetic models such as First- and Second-Order Kinetics, the Langmuir-Hinshelwood model, and the two-parameter Weibull distribution.

Keywords: Copper Nanoferrite, Photocatalytic Degradation, Methylene Blue, Kinetics Fitting; Langmuir-Hinshelwood model; Weibull distribution model.

Received 11 June 2024; Accepted 19 September 2024.

Introduction

Copper ferrite ($CuFe_2O_4$), like other spinel ferrites, is highly effective, particularly as a photocatalyst for degrading organic dyes in aqueous solutions [1, 2]. However, pure copper ferrite undergoes a phase transformation from cubic (Fd3m) to tetragonal (I_4/amd) [3] due to Jahn-Teller distortion [4] under varying external conditions, such as elevated temperature [5] and pressure [6], which can significantly alter its properties.

This phase transformation can be suppressed [7] by substituting a portion of the copper ions with other ions, such as magnesium. Spinel nanoparticles of copper ferrites can be synthesized using various methods, including self-organized high-temperature synthesis (HTS) [8], deposition from a polymer matrix [9, 10], citrate eco-composition [11], coprecipitation [12], hydrothermal crystallization [13], low-temperature reactions [14], sol-gel processing [15], and microwave synthesis [16]. These studies demonstrated that the crystallite size, morphology, and phase composition of $CuFe_2O_4$ and substituted $CuFe_2O_4$ highly depend on the synthesis method. However, achieving the desired outcomes can be challenging, primarily because the magnetic properties of the nanoparticles lead to a strong tendency for aggregation [3], often resulting in suboptimal results.

The sol-gel combustion method appears promising in this study due to its simplicity and the ability to precisely control the properties of the final product [17]. To further enhance the process, citric acid—commonly used as a chelating agent in synthesis – was substituted with polyethylene glycol with molar weight M_W = 2000 (PEG-2000). PEG-2000 offers several advantages, including

improved particle dispersion and reduced aggregation, leading to better control over particle size and morphology [18]. Additionally, PEG helps to avoid unwanted side reactions that can occur with citric acid. However, there is limited information in the current literature regarding the impact of using PEG-2000 instead of citric acid on the elastic properties of the resulting nanoparticles, making this a novel aspect of the study.

This study aims to investigate the influence of using PEG-2000 as both a fuel and chelating agent on the morphology, structural, and elastic properties of magnesium ion-substituted copper ferrites synthesized via the sol-gel autocombustion method. The substitution of traditional chelating agents like citric acid with PEG-2000 is expected to offer enhanced control over nanoparticle formation, reduce aggregation, and potentially improve the material's overall performance. Understanding how PEG-2000 affects these fundamental properties is critical for optimizing the synthesis process and tailoring the material for specific applications, such as photocatalysis or magnetic devices.

I. Synthesis and characterization techniques

The synthesis process began with the selection of chemical precursors, including iron nitrate nonahydrate ($Fe(NO_3)_3 \cdot 9H_2O$), copper nitrate trihydrate ($Cu(NO_3)_2 \cdot 3H_2O$), and magnesium nitrate hexahydrate ($Mg(NO_3)_2 \cdot 6H_2O$), all supplied by LobaChemi, India. Additionally, polyethylene glycol (PEG 2000), obtained from Carl Roth GmbH, Germany, acted as a chelating agent. The use of PEG not only facilitated the uniform distribution of the metal ions but also contributed to controlling the size and morphology of the nanoparticles.

The nanoparticles were synthesized using the sol-gel autocombustion technique, as described in detail in [18], the metal nitrates were mixed in stoichiometric proportions, ensuring the correct ratio of Mg^{2+}, Cu^{2+}, and Fe^{3+} ions for the desired ferrite composition. The solid precursors were dissolved in distilled water, and the resulting solution was stirred continuously to achieve a homogenous mixture.

Once the solution was fully mixed, it underwent a drying process to remove the water content. The drying was carried out under controlled conditions until all the water had evaporated, leaving behind a gel-like substance known as xerogel. This xerogel was then transferred to a preheated oven set between 250°C and 300°C. At this elevated temperature, the remaining moisture was eliminated, and the xerogel spontaneously ignited. This self-ignition marked the start of an exothermic combustion reaction, which proceeded rapidly, resulting in the formation of a lightweight, highly porous material.

For each sample, chemical composition and crystal structure were determined using XRD measurements in a PANalytical X'Pert Empyrean Series Bragg − Brentano powder diffractometer (United Kingdom) with a radius of 240 mm using Cu Kα radiation (λ = 1.5418 Å) in the 10–70° 2θ range and a scan step of 0.013 for 2 s. The attenuated total reflection Fourier transform infrared (ATR-FTIR) spectra were recorded in the 4000–300 cm^{-1} range on a Bruker VERTEX 70v Fourier transform infrared spectrometer (Germany) with ATR. A resolution of 4 cm−1 was used to obtain all the spectra. The room temperature VSM measurements for all samples were collected in LakeShore Model 7407 (United States) vibrating sample magnetometer (VSM) with an oven under an argon atmosphere (6 N). Optical and photocatalytic studies were performed on the ULAB 108UV spectrophotometer (Ukraine).

II. Results and discussion.

2.1. X-ray diffraction studies

Figure 1 presents the X-ray diffraction patterns of magnesium-substituted copper nanoferrite samples synthesized using the sol-gel autocombustion method [19], with PEG-2000 as fuel.

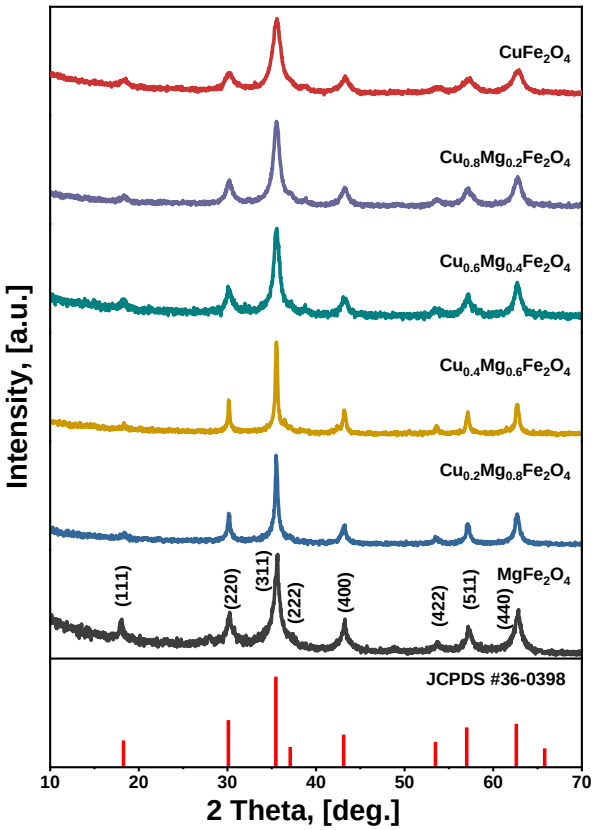

Fig. 1. Experimental X-ray diffraction patterns of magnesium-substituted copper ferrites synthesized by the sol-gel autocombustion method using PEG-2000 as fuel.

The characteristic peaks at 2θ angles of 30.3°, 35.7°, 37.3°, 43.3°, 53.7°, 57.3°, and 62.9° correspond to the (220), (311), (222), (400), (422), (333), and (440) crystallographic planes, respectively. According to the Joint Committee on Powder Diffraction Standards (JCPDS) card numbers 25-0283 for $CuFe_2O_4$ and 36-0398 for $MgFe_2O_4$, these peaks are consistent with the cubic spinel structure of the Fd3m space group [20- 22]. The absence of additional peaks indicates that no impurity phases are present. As the magnesium content increases, the diffraction peaks become sharper and narrower, suggesting an increase in particle size. This is likely due to the catalytic effect of magnesium, which leads to a

higher temperature during the synthesis process. The variation in the lattice constant as a function of magnesium ion content is depicted in Fig. 2.

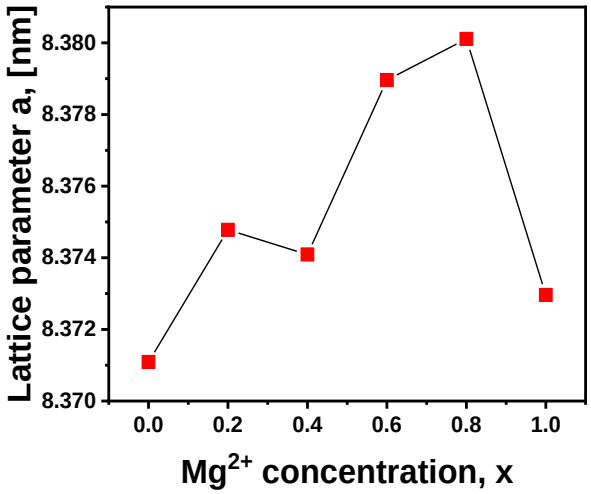

Fig. 2. Dependence of the lattice constant on the magnesium ion content.

As the magnesium content increases, the lattice constant also increases. This is because copper ions, with a smaller ionic radius (0.72 Å), are replaced by magnesium ions, which have a larger ionic radius (0.78 Å), consistent with Vegard's law [23]. Due to the small particle size, approximately 10 nm, a noticeable scattering of data points is expected.

Table 1 presents the main structural characteristics of the synthesized ferrites.

The dislocation density can be calculated using the Williamson and Smallman formula, $\delta = 1/D^2$ [24, 25], while the number of unit cells per particle is determined by the formula $n = (\pi \cdot D^3)/6V$. As shown in table 1, dislocation density is inversely proportional to particle size, while the number of unit cells increases linearly with particle size. This indicates that as particle size increases, dislocation density decreases, suggesting an improvement in particle crystallinity. This can be explained by the fact that the surface-to-volume ratio increases as particle size decreases. Since various defects, including dislocations, tend to accumulate at the particle surface, smaller particles experience a higher contribution from surface defects, leading to increased dislocation density.

2.2. Optical Studies

The Tauc plot is a widely used method to estimate the optical band gap (E_g) of semiconductors and insulating materials from their UV-Vis absorption spectrum [26, 27]. This method is based on the Tauc relation, which connects the absorption coefficient of a material to the photon energy. The Tauc plot helps determine the energy of electronic transitions from the valence band to the conduction band, giving insight into the material's optical properties.

The absorption coefficient (α) in semiconductors describes how much light is absorbed as it passes through the material. Near the absorption edge, the absorption coefficient is related to the photon energy (hν) by the equation

$$\alpha h\nu = A\left(h\nu - E_g\right)^n$$

where A is a constant, Eg is the optical band gap, and n is an exponent that depends on the type of electronic transition. For direct allowed transitions, n=1/2, while for indirect allowed transitions, n=2. The exponent varies for other types of transitions, such as forbidden transitions.

The Tauc relation allows for the graphical determination of the optical band gap by plotting $(\alpha h\nu)^n$ against hν. The Tauc plot is typically represented as $(\alpha h\nu)^n$ vs hν.

In this plot, the linear region near the absorption edge is extrapolated to the x-axis (where α=0) to find the intercept, corresponding to the optical band gap (Eg).

Figure 3 presents the plot of $(\alpha h\nu)^2$ against hν for $Cu_{1-x}Mg_xFe_2O_4$ nanoparticles, calculated from their UV-Vis absorption data using Tauc's equation.

2.3. Photocatalytic Studies

Photocatalytic degradation of organic dyes has gathered significant attention as an efficient and environmentally friendly approach for wastewater treatment. Among these dyes, Methylene Blue (MB), commonly used in textile and paper industries, poses a severe environmental threat due to its toxicity and persistence in aquatic ecosystems [29]. Nanostructured materials, particularly spinel ferrites, have shown promise as photocatalysts for

Table 1.

Structural and morphological characteristics of magnesium-substituted copper ferrites synthesized by the sol-gel autocombustion method using PEG-2000 as fuel.

Sample	Cubic phase, %	Crystallites size D, nm	Lattice constant a, nm	Lattice strain	Cell volume V, nm	X-Ray density	The number of elementary cells, $n \cdot 10^3$	Density of dislocations, δ 10^{18}/м^2
x = 0.0	100	8	8.3710	0.017	586.6	5.437	0.38	0.0181
x = 0.2	100	9	8.3747	0.012	587.3	5.411	0.59	0.0132
x = 0.4	100	10	8.3740	0.014	587.2	5.412	0.97	0.0094
x = 0.6	100	21	8.3789	0.003	588.2	5.403	7.76	0.0024
x = 0.8	100	19	8.3801	0.005	588.5	5.400	6.20	0.0027
x = 1.0	100	12	8.3729	0.011	586.9	5.414	1.70	0.0065
errors	±0.1	±1	±0.0001	±0.001	±0.1	±0.01	±0.01	±0.0001

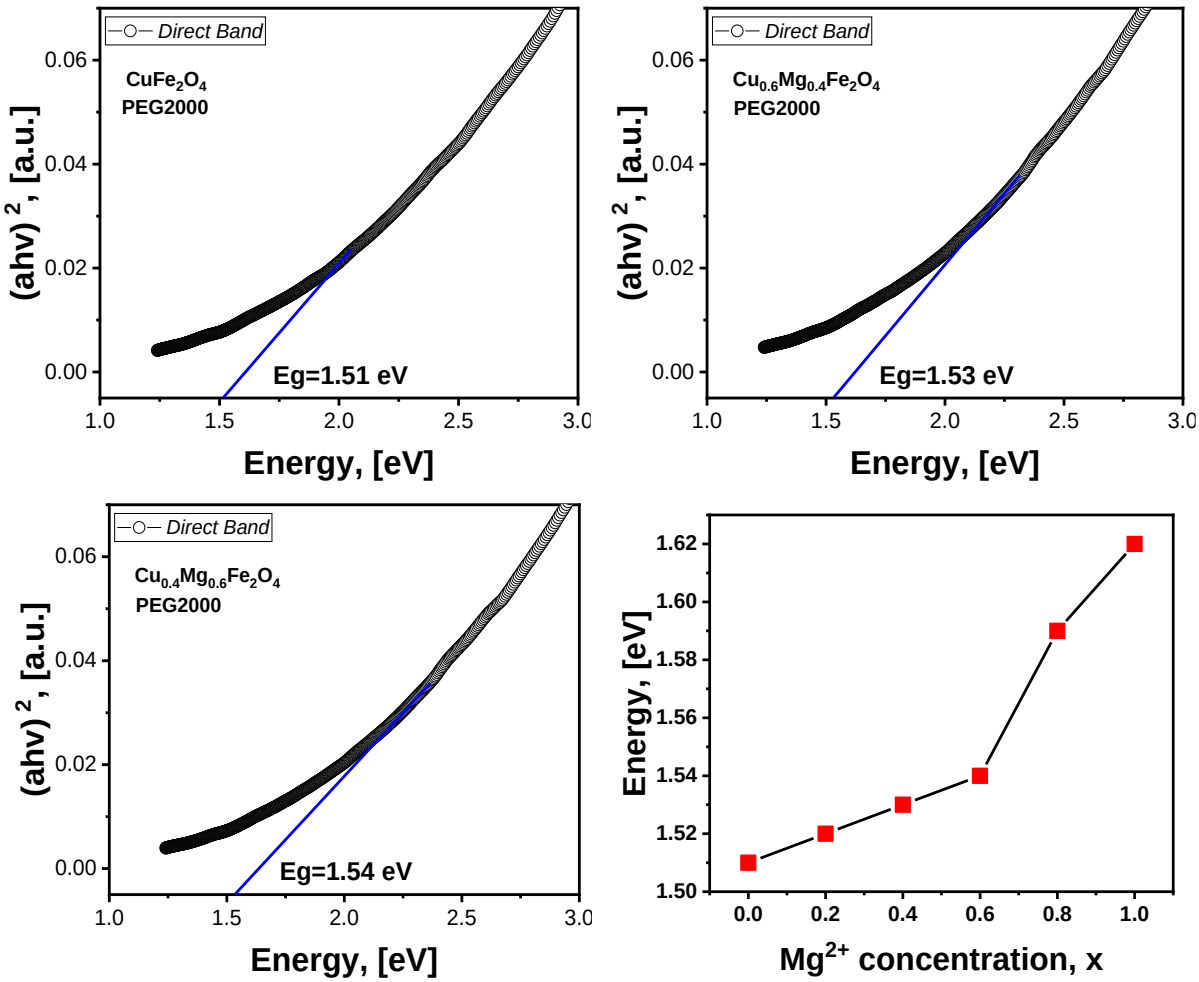

Fig. 3. Plots of $(\alpha h\nu)^2$ against hν for $Cu_{1-x}Mg_xFe_2O_4$ nanoparticles were calculated from their UV-Vis absorption data using Tauc's equation.

the degradation of such dyes under visible light irradiation [30]. In this context, $Cu_{1-x}Mg_xFe_2O_4$ nanoparticles offer a unique combination of magnetic and optical properties that make them suitable for photocatalytic applications. The substitution of copper with magnesium is expected to enhance photocatalytic efficiency by tuning the band gap and improving charge separation.

The photocatalytic activity of $Cu_{1-x}Mg_xFe_2O_4$ nanoparticles for Methylene Blue (MB) dye (fig. 4) degradation was evaluated under visible light irradiation.

The experimental setup involved preparing an aqueous solution of Methylene Blue with a concentration of 10 mg/L. 0.15g of $Cu_{1-x}Mg_xFe_2O_4$ nanoparticles and 3.5ml of H_2O_2 were added to 100 mL of the dye solution, and the mixture was magnetically stirred in the dark for 30 minutes to ensure adsorption-desorption equilibrium between the catalyst and the dye molecules.

After this initial period, the reaction vessel was exposed to visible light using a 150 W halogen lamp to simulate solar light. The distance between the light source and the solution was maintained at 10 cm. During the photocatalytic reaction, 5 mL samples were withdrawn at intervals (every 20 minutes) for up to 200 minutes.

The degradation of Methylene Blue was tracked by recording the absorbance of the samples using a UV-Vis spectrophotometer, with the absorbance intensity measured at the characteristic wavelength of MB

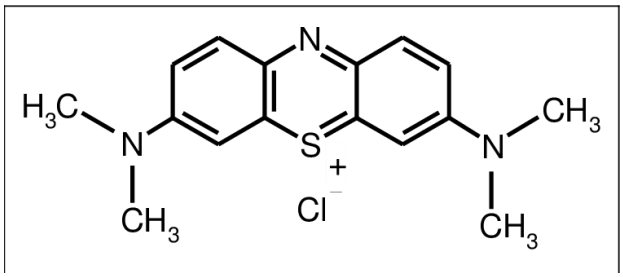

Fig. 4. Chemical structure of Methylene Blue.

(~665 nm). All experiments were carried out at room temperature.

The photocatalytic degradation of Methylene Blue (MB) under visible light in the presence of ferrite powder and hydrogen peroxide (H_2O_2) involves a synergistic process where both the photocatalyst and the oxidizing agent contribute to the breakdown of the dye molecules. Ferrite nanoparticles act as photocatalysts by absorbing visible light and generating electron-hole pairs. H_2O_2 further enhances this process by serving as an additional source of reactive oxygen species (ROS), such as hydroxyl radicals (OH), which play a crucial role in oxidizing the dye molecules.

In the experimental setup, when the ferrite nanoparticles are exposed to visible light, they absorb photons hν with energy greater than or equal to their band

gap, creating electron-hole pairs:

$$Ferrite + hv \rightarrow e_{CB}^{-} + h_{VB}^{+}$$

Here, e_{CB}^{-} represents the excited electron in the conduction band and h_{VB}^{+} is the hole in the valence band.

The electrons in the conduction band react with dissolved oxygen to form superoxide radicalsO_2^-:

$$O_2 + e_{CB}^{-} \rightarrow O_2^{-}$$

The holes in the valence band can oxidize water molecules or hydroxide ions (\(OH^-\)) to produce hydroxyl radicals OH:

$$H_2O + h_{VB}^{+} \rightarrow OH + H^{+}$$

$$OH^{-} + h_{VB}^{+} \rightarrow OH$$

The introduction of H_2O_2 enhances the production of hydroxyl radicals. Hydrogen peroxide can decompose through multiple pathways:

- Reduction by conduction band electrons:

$$H_2O_2 + e_{CB}^{-} \rightarrow OH + OH^{-}$$

- Reaction with superoxide radicals:

$$H_2O_2 + O^{-} \rightarrow OH + OH^{-} + O_2$$

The hydroxyl radicals OH and superoxide radicals O_2^- produced in these reactions attack the Methylene Blue (MB) molecules, breaking them down into smaller, less harmful products like water and various gases (fig. 5).

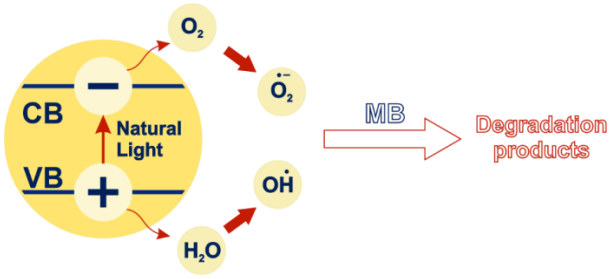

Fig. 5. Reaction mechanism of Methylene Blue photodegradation over ferrite nanoparticles under natural light irradiation.

Figure 6 particularly highlights systems with magnesium substitution levels (x = 0.0), (x = 0.4), and (x=0.6), showing the change in relative (C/C_0) concentration over the illumination period for all photocatalyst systems. As illustrated in the figure 6, the sample with no magnesium substitution (x=0.0), $CuFe_2O_4$, exhibits the most rapid degradation, reaching near-complete degradation with a final (C/C_0) value of 0.05026 at 160 minutes, indicating its superior photocatalytic efficiency.

On the other hand, samples with magnesium substitution levels of (x=0.4) and (x=0.6) also demonstrate excellent degradation capabilities. The (x=0.4) system reaches a final degradation level with (C/C_0=0.2223) by 180 minutes, while the (x=0.6) system degrades to (C/C_0=0.3267) by 160 minutes. These results reflect the

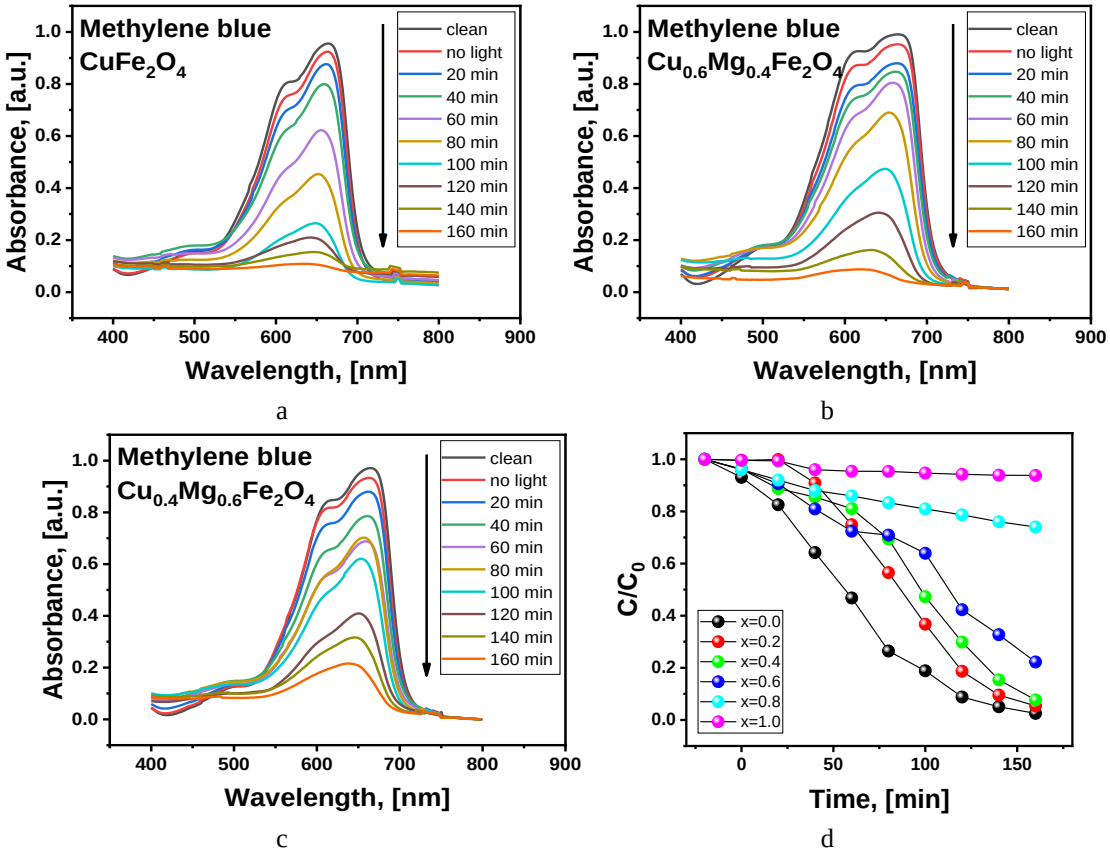

Fig. 6. Photocatalytic Degradation profiles of Methylene Blue (MB) for $Cu_{1-x}Mg_xFe_2O_4$ ferrites with x ranging from 0.0 to 1.0; (d) shows the C/C_0 as a function of irradiation time.

impact of magnesium substitution on the photocatalytic activity of the system, with moderate Mg levels still promoting significant degradation, though at a slower rate compared to pure $CuFe_2O_4$.

In the context of heterogeneous catalysis, such as those involving ferrites in the Fenton photoreaction, magnesium substitution influences the surface and electronic properties of the catalyst, affecting charge carrier mobility and recombination rates. Mathematical modeling is often employed to describe the kinetics of such systems. Models such as the Langmuir-Hinshelwood mechanism are widely used to interpret the photocatalytic degradation of organic pollutants, as they account for surface adsorption, reaction rate, and photon absorption. In these ferrite systems, the degradation kinetics may also be governed by factors like particle size, bandgap modification due to doping, and the availability of active sites.

2.3.1. First and Second-order kinetics fitting

The First-Order Kinetics Model (fig. 7) is the most widely used model for photocatalytic degradation [31, 32], assuming that the reaction rate is proportional to the dye concentration.

$$\ln\left(\frac{C_0}{C}\right) = kt$$

Where C_0 - initial concentration of the dye; C – concentration of the dye at time t; k – first-order rate constant (min^{-1}); t – time.

If the reaction follows first-order kinetics, the plot will be linear, and the slope will give the rate constant k.

Suppose the degradation does not fit first-order kinetics. In that case, it is possible to test second-order kinetics [31, 33] (fig. 7), which assumes the reaction rate depends on the square of the dye concentration.

$$\frac{1}{C} = kt + \frac{1}{C_0}$$

Where C_0 - initial concentration of the dye; C - concentration of the dye at time t; k - second-order rate constant (L/mol·min); t - time.

To quantitatively compare the models, the following statistical metrics were calculated to help assess the fit quality (table 2): Sum of Squared Residuals (SSR) - this measures the total squared difference between the experimental data and the fitted model. The smaller the SSR, the better the fit; R^2 (Coefficient of Determination) is a standard measure of how well a model explains the variability in the data. An R^2 value closer to 1 indicates a better fit.

The First-order kinetics assumes that the degradation rate depends linearly on the concentration of the reactant (dye). This is common for reactions with sufficient availability of the reactant and catalyst, and the reaction progresses uniformly. In comparison, the Second-Order kinetics implies that the reaction rate depends on the square of the concentration. This is more typical in systems where interactions between molecules (e.g., collisions) become essential.

Across all samples, the Second-Order Kinetics model consistently provided a better fit to the experimental data, suggesting that these photocatalytic reactions do not follow simple first-order behavior. Instead, they are likely run by second-order processes, where the rate depends on the concentrations of multiple reactants or intermediates, possibly due to surface interactions with the catalyst.

This analysis points to complex reaction mechanisms for ferrite-based photocatalysts, where adsorption, interactions between species, and catalyst surface effects significantly influence the overall reaction rates.

2.3.2. Langmuir-Hinshelwood model

The Langmuir-Hinshelwood model [34, 35] is commonly used to describe photocatalytic degradation reactions when the adsorption of the reactants on the photocatalyst surface plays a significant role. It combines the concepts of adsorption and surface reaction, making it highly relevant for systems where reactants (such as dyes in solution) must adsorb onto the surface of a catalyst before undergoing degradation.

According to this model, the reactant (dye molecules) must first adsorb onto the surface of the photocatalyst. After adsorption, the degradation reaction occurs on the

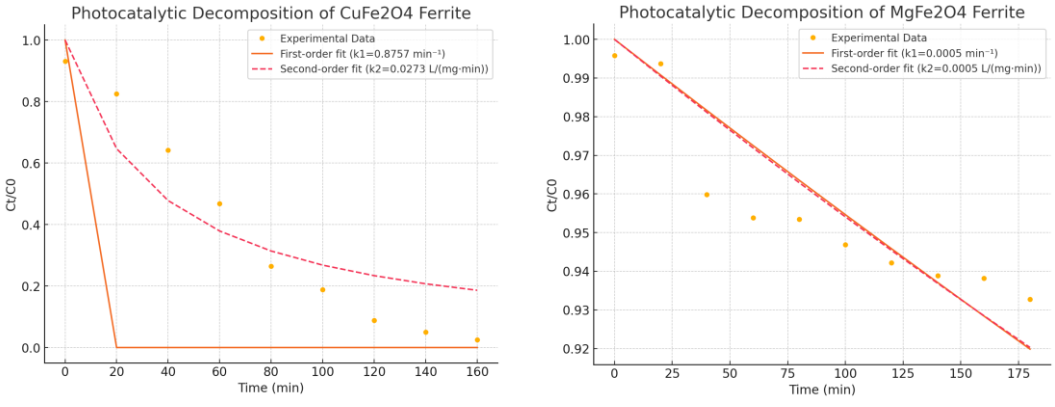

a b

Fig. 7. Comparison of first-order and second-order kinetic model fittings for the photocatalytic degradation of Methylene Blue for (a) $CuFe_2O_4$ and (b) $MgFe_2O_4$ samples. The black crosses represent the experimental data (relative concentration C/C0) obtained from absorbance measurements over time. Model fitting was performed using the *Python* programming language, using the following libraries: *Numpy* for numerical calculations and array manipulation; *Pandas* for data organization and manipulation; *Matplotlib* for plotting the experimental data and the model fit; *Scipy* (*curve_fit*) for fitting the experimental data to the first-order and second-order kinetic models.

Table 2.

Comparison of First-Order and Second-Order Kinetic model fittings for the photocatalytic degradation of Methylene Blue on $Cu_{1-x}Mg_xFe_2O_4$ ferrite nanoparticles.

Sample	Statistical metric	First-Order Model	Second-Order Model
$CuFe_2O_4$	**SSR** (Sum of Squared Residuals)	1.4333	0.1523
	R^2 (Coefficient of Determination)	-0.5122	0.8393
$Cu_{0.8}Mg_{0.2}Fe_2O_4$	**SSR** (Sum of Squared Residuals)	2.8845	0.3306
	R^2 (Coefficient of Determination)	-1.4307	0.7214
$Cu_{0.6}Mg_{0.4}Fe_2O_4$	**SSR** (Sum of Squared Residuals)	2.5036	0.2570
	R^2 (Coefficient of Determination)	-1.7581	0.7170
$Cu_{0.4}Mg_{0.6}Fe_2O_4$	**SSR** (Sum of Squared Residuals)	1.7295	0.0967
	R^2 (Coefficient of Determination)	-1.6469	0.8188
$Cu_{0.2}Mg_{0.8}Fe_2O_4$	**SSR** (Sum of Squared Residuals)	2.0713	0.0046
	R^2 (Coefficient of Determination)	-1.0121	0.8926
$MgFe_2O_4$	**SSR** (Sum of Squared Residuals)	0.0012	0.0012
	R^2 (Coefficient of Determination)	0.7111	0.7583

catalyst surface, often initiated by light (in photocatalysis). The degradation rate depends on the concentration of the reactant adsorbed on the catalyst surface rather than in the bulk solution.

The general form of the Langmuir-Hinshelwood (fig. 8) model is [34]:

$$r = \frac{k_{L-H}K_{ads}C}{1+K_{ads}C} \quad (24)$$

Where r – reaction rate (rate of degradation of the reactant); k_{L-H} – intrinsic rate constant for the surface reaction; K_{ads} – adsorption equilibrium constant (how strongly the reactant adsorbs onto the catalyst surface); C – concentration of the reactant (e.g., dye) in the solution.

The experimental photocatalytic degradation data were successfully fitted (table 3) to the Langmuir-Hinshelwood (L-H) model, widely used to describe heterogeneous catalytic processes. The model demonstrated an adequate representation of the photocatalytic kinetics in each case, showing the relationship between reaction rates and adsorption equilibrium constants.

$Cu_{0.8}Mg_{0.2}Fe_2O_4$ and $Cu_{0.4}Mg_{0.6}Fe_2O_4$ samples have the highest reaction rate and adsorption constant, indicating that the Mg substitution enhances the overall photocatalytic performance. The strong adsorption capacity combined with faster degradation of pollutants highlights the potential of Mg-substituted ferrites in photocatalytic applications.

Adding magnesium ions to the ferrite structure significantly improves the adsorption of reactants and the photocatalytic reaction rates. Among the tested materials, $Cu_{0.8}Mg_{0.2}Fe_2O_4$ and $Cu_{0.4}Mg_{0.6}Fe_2O_4$ samples stand out as the most efficient photocatalyst, indicating that the substitution of copper by magnesium enhances photocatalytic properties, likely due to changes in surface properties and the electronic structure of the ferrite.

2.3.3. Weibull distribution model

The two-parameter Weibull distribution model [36] is commonly used to describe the kinetics of complex processes where the degradation (i.e., investigated process) does not follow simple exponential decay (as in first-order kinetics). In photocatalytic degradation, the Weibull model can account for different reaction stages, such as an initial rapid phase followed by a slower one.

The general form of the Weibull distribution model (fig. 9) for degradation processes is:

$$C(t) = C_0 \exp\left(-(kt)^m\right)$$

Where C(t) is the concentration of the reactant (e.g., dye) at time t; C_0 is the initial concentration (at t=0); k is the rate constant (min^{-1}), controlling the speed of the reaction; m is the shape parameter, which controls the curve shape and describes how the reaction progresses over time.

The Weibull model is beneficial for systems where simple first- or second-order kinetics do not apply, often due to complexities in the degradation mechanism. For instance, several processes (adsorption, diffusion, chemical reaction, etc.) might coincide in photocatalysis, leading to deviations from simpler kinetic models. The model parameters (table 3) — k (rate constant) and m (shape parameter) — allowed for a detailed comparison of the degradation processes among different compositions. The shape parameter m provided an understanding of how the degradation rate evolves, whether it accelerates or remains relatively constant.

If *m=1:* The reaction follows first-order kinetics (simple exponential decay).

If *m>1:* The reaction proceeds more slowly at first and then speeds up over time (accelerating process).

If *m<1:* The reaction starts fast but slows down over time (decelerating process).

Mg-substituted copper ferrites exhibit accelerated photocatalytic degradation, increasing the degradation rate as more Mg is substituted into the system. $Cu_{0.6}Mg_{0.4}Fe_2O_4$ and $Cu_{0.8}Mg_{0.2}Fe_2O_4$ show the highest degradation rates, making them highly effective photocatalysts. In contrast, pure $MgFe_2O_4$ demonstrates a much slower and more constant degradation process, indicating that Cu substitution significantly enhances photocatalytic activity.

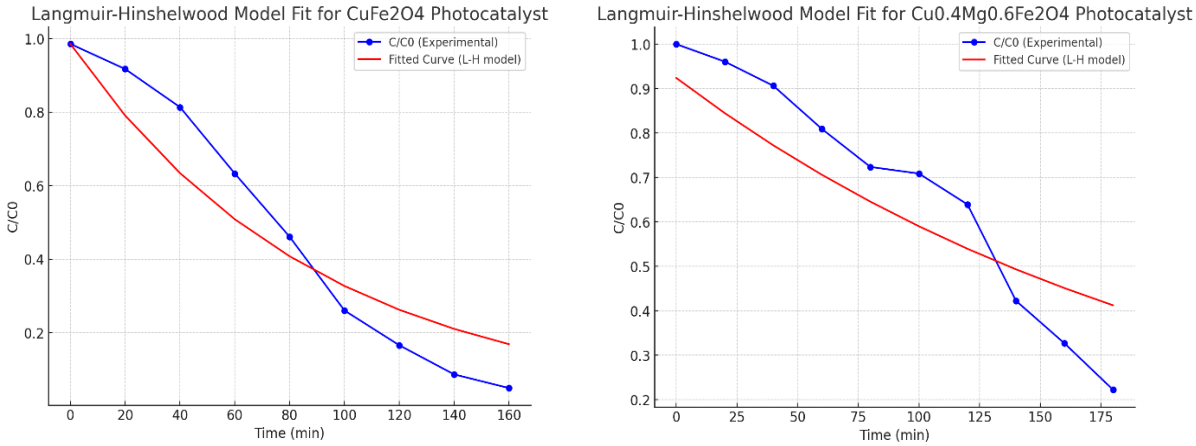

Fig. 8. Fitting the experimental photocatalytic degradation data of Methylene Blue on (a) $CuFe_2O_4$ and (b) $Cu_{0.4}Mg_{0.6}Fe_2O_4$ samples to the Langmuir-Hinshelwood model. The blue points represent the experimental data (relative concentration (C/C_0)) obtained from absorbance measurements over time, and the red line represents the Langmuir-Hinshelwood model fit. Model fitting was performed using the *Python* programming language, using the following libraries: *Numpy* for numerical calculations and array manipulation; *Pandas* for data organization and manipulation; *Matplotlib* for plotting the experimental data and the model fit; *Scipy* (*curve_fit*) for nonlinear curve fitting to optimize the kinetic parameters.

Table 3.

Fitting the experimental photocatalytic degradation data of Methylene Blue on $Cu_{1-x}Mg_xFe_2O_4$ ferrite nanoparticles to the Langmuir-Hinshelwood and Weibull distribution models.

Sample	Langmuir-Hinshelwood model		Weibull distribution model	
	Reaction rate constant, k_{L-H}, min^{-1}	Adsorption equilibrium constant, Kads	Rate constant, k (min^{-1})	Shape parameter, m
$CuFe_2O_4$	0.2203	21.1474	$1.11 \cdot 10^{-2}$	2.0413
$Cu_{0.8}Mg_{0.2}Fe_2O_4$	0.3583	58.1879	$8.37 \cdot 10^{-3}$	3.0658
$Cu_{0.6}Mg_{0.4}Fe_2O_4$	0.2317	44.4870	$7.42 \cdot 10^{-3}$	3.3658
$Cu_{0.4}Mg_{0.6}Fe_2O_4$	0.3455	84.7790	$6.36 \cdot 10^{-3}$	2.2654
$Cu_{0.2}Mg_{0.8}Fe_2O_4$	0.1531	40.1872	$4.21 \cdot 10^{-3}$	2.0125
$MgFe_2O_4$	0.0200	42.3600	$4.54 \cdot 10^{-4}$	0.9525

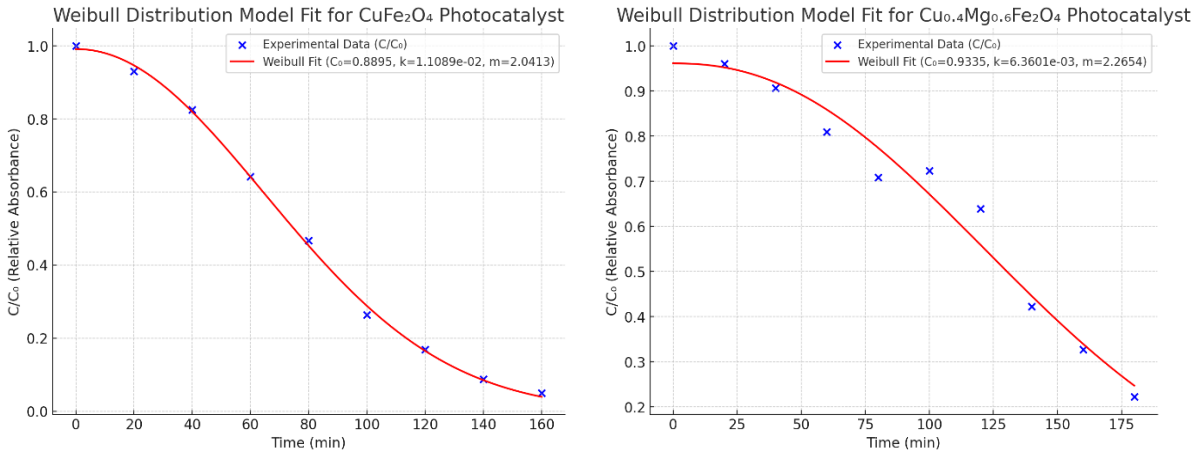

Fig. 9. F Fitting the experimental photocatalytic degradation data of Methylene Blue on (a) $CuFe_2O_4$ and (b) $Cu_{0.4}Mg_{0.6}Fe_2O_4$ samples to the Weibull distribution model. The blue points represent the experimental data (relative concentration C/C0) obtained from absorbance measurements over time, and the green line represents the Weibull model fit. The Weibull model fitting was performed using the *Python* programming language, leveraging the following libraries: *Numpy* for numerical calculations and array manipulation; *Pandas* for data organization and manipulation; *Matplotlib* for plotting the experimental data and the Weibull model fit; *Scipy* (*curve_fit*) for nonlinear curve fitting to optimize the parameters k and m of the Weibull model.

Conclusions

In this study, a system of magnesium-substituted copper ferrites was developed using the sol-gel autocombustion method with polyethylene glycol (PEG-2000) as fuel. The investigation focused on the effect of replacing the chelating agent on the structural, elastic, and magnetic properties of the material. All synthesized systems were identified as single-phase cubic spinel with the space group Fd3m, with no impurity phases detected. It was demonstrated that using PEG-2000 as both fuel and chelating agent led to a significant reduction in particle size to 7-10 nm, in contrast to the traditional use of citric acid, which typically produces particles of 25-40 nm.

With an increase in magnesium ion content, the lattice constant increased due to substituting smaller ions with larger ones. The dislocation density was inversely proportional to the particle size, while the number of unit cells showed a direct relationship. As particle size increased, the dislocation density decreased, indicating improved crystallinity. Conversely, a decrease in particle size resulted in an increased surface-to-bulk ratio, leading to a rise in dislocation density due to smaller particles' more significant surface contribution.

The optical studies of ferrite samples reveal that the band gaps, determined from Tauc plots, range from 1.51 eV to 1.62 eV. This increase in the band gap is observed as the composition shifts from $CuFe_2O_4$ to $MgFe_2O_4$, indicating that magnesium substitution leads to a widening of the band gap. This trend suggests that the ferrite's electronic structure is modified by replacing copper ions with magnesium ions, resulting in reduced electronic transition energies. The observed band gap values indicate that all samples remain within the range typical for semiconductors, making them suitable for potential applications in photocatalysis.

The photocatalytic studies demonstrate that the $CuFe_2O_4$ sample exhibits the most efficient degradation of Methylene Blue organic dye, achieving near-complete degradation with a final (C/C_0) value of 0.05026 at 160 minutes. This indicates its superior photocatalytic efficiency. Samples with magnesium substitution ($x = 0.4$) and ($x = 0.6$) also show significant degradation capabilities, with ($x = 0.4$) reaching a (C/C_0) value of 0.2223 by 180 minutes and ($x = 0.6$) reaching 0.3267 by 160 minutes.

These results indicate that magnesium substitution still promotes photocatalytic activity but reduces the degradation rate compared to pure $CuFe_2O_4$. The findings suggest that magnesium influences the surface and electronic properties, impacting charge carrier mobility and recombination rates, which are critical for efficient photocatalysis.

The First-Order Kinetics model showed a poor fit across all samples. In contrast, the Second-Order Kinetics model provided a better fit, suggesting the reactions are governed by second-order processes, likely due to surface interactions with the catalyst. The Langmuir-Hinshelwood (L-H) model well-represented the photocatalytic degradation data, linking reaction rates to adsorption constants. $Cu_{0.8}Mg_{0.2}Fe_2O_4$ and $Cu_{0.4}Mg_{0.6}Fe_2O_4$ exhibited the highest reaction rates and adsorption capacity, indicating that Mg substitution enhances photocatalytic performance by improving surface properties and electronic structure.

The Weibull model further revealed that Mg substitution accelerates degradation, with $Cu_{0.6}Mg_{0.4}Fe_2O_4$ and $Cu_{0.8}Mg_{0.2}Fe_2O_4$ showing the fastest degradation rates, making them highly effective photocatalysts. In contrast, pure $MgFe_2O_4$ showed slower, constant degradation toward Methylene Blue organic dye, highlighting the significant role of copper in boosting photocatalytic activity.

Funding:

This work was funded by the Narodowa Agencja Wymiany Akademickiej (Grant Ulam NAWA: BPN/ULM/2022/1/00093) and partly supported by a grant 0124U001654 of the Ministry of Education and Science of Ukraine.

Acknowledgments:

The authors are grateful to the Narodowa Agencja Wymiany Akademickiej for financial support. The authors thank the Ministry of Education and Science of Ukraine for grants for implementing project 0124U001654. The authors express their sincere gratitude and respect to the Armed Forces of Ukraine, who made it possible to complete the preparation of this article for publication. The team of authors expresses their gratitude to the reviewers for valuable recommendations that have been considered to improve the quality of this paper significantly.

Mazurenko Julia **–** Candidate of Physical and Mathematical Sciences (Ph.D.), Associate Professor (Docent) at the Department of Medical Informatics, Medical and Biological Physics, Ivano-Frankivsk National Medical University, Researcher at the Faculty of Physics and Applied Computer Science, AGH University of Krakow;
Kaykan Larysa – Doctor of Physical and Mathematical Sciences, Senior Researcher at the Laboratory for Physics of Magnetic Films, G.V. Kurdyumov Institute for Metal Physics, N.A.S. of Ukraine;
Moklyak Volodymyr – Doctor of Physical and Mathematical Sciences, Professor, Head of Laboratory for Physics of Magnetic Films, G.V. Kurdyumov Institute for Metal Physics, N.A.S. of Ukraine, Professor of the Department of Physical and Mathematical Sciences, Ivano-Frankivsk National Technical University of Oil and Gas.;
Petryshyn Mykhailo **–** Candidate of Technical Sciences (Ph.D.), Associate Professor at the Department of Computer Science, Vasyl Stefanyk Precarpathian National University;
Mazurenko Oleksandr – BSc student, Department of Computer Science, Vasyl Stefanyk Precarpathian National University;
Leleko Sofiia – medical student, Medical Faculty, Ivano-Frankivsk National Medical University.

[1] P.A. Udhaya, A. Ahmad, M. Meena, M.A.J. Queen, M. Aravind, P. Velusamy, T.M. Almutairi, A.A.A. Mohammed, S. Ali, *Copper Ferrite Nanoparticles Synthesized Using a Novel Green Synthesis Route: Structural Development and Photocatalytic Activity*, Journal of Molecular Structure, 1277, 134807 (2023); https://doi.org/10.1016/j.molstruc.2022.134807.

[2] N.A.H. Mohammed, R. N. Shamma, S. Elagroudy, A. Adewuyi, *Copper Ferrite Immobilized on Chitosan: A Suitable Photocatalyst for the Removal of Ciprofloxacin, Ampicillin and Erythromycin in Aqueous Solution*, Catalysis Communications, 182, 106745 (2023); https://doi.org/10.1016/j.catcom.2023.106745.

[3] J.A. Jaén, M. Coronado, E. Chung, A. Muñoz, M. Denvers, G. Caballero-Manrique, *Structural and Electrochemical Characterization of Tetragonal Copper Ferrite Nanoparticles*, Interactions, 245(1) (2024); https://doi.org/10.1007/s10751-024-01848-7.

[4] M.Á. Cobos, J.A. Jiménez, I. Llorente, P. de la Presa, A. Hernando, *Ball Milling and Annealing Effect in Structural and Magnetic Properties of Copper Ferrite by Ceramic Synthesis*, Journal of Alloys and Compounds, 1006, 176206 (2024); https://doi.org/10.1016/j.jallcom.2024.176206.

[5] R. Rajini, A. Christy Ferdinand, *Effects of Annealing on the Structural, Morphological and Magnetic Properties of $CuFe_2O_4$ Ferrite Nanoparticles Synthesized by Chemical Precipitation*, Chemical Data Collections, 44, 100985 (2023); https://doi.org/10.1016/j.cdc.2022.100985.

[6] A. Sivakumar, S.S.J. Dhas, A.I. Almansour, R.S. Kumar, N. Arumugam, A.M.B.S. Dhas, *Assessment of Crystallographic and Magnetic Phase Stabilities of Cubic Copper Ferrite at Shocked Conditions*, Journal of Materials Science: Materials in Electronics, 32(9), 12732 (2021); https://doi.org/10.1007/s10854-021-05910-w.

[7] K.N. Harish, S. Reddy, M.S. Dharmaprakash, S. Chapi, B.S. Surendra, H.S. Bhojya Naik, B. Vinay Kumar, A. V. Raghu, *Solar Photoactive Magnesium Substituted Copper Ferrite Photocatalysts for Rose Bengal Treatment*, Results in Chemistry, 7, 101246 (2024); https://doi.org/10.1016/j.rechem.2023.101246.

[8] H.-C. Lu, J.-E. Chang, P.-H. Shih, & L.-C. Chiang, *Stabilization of copper sludge by high-temperature CuFe2O4 synthesis process.* Journal of Hazardous Materials 150(3), 504 (2008); https://doi.org/10.1016/j.jhazmat.2007.04.130.

[9] K.A. Hamzah, C.K. Yeoh, M.M. Noor, P.L. Teh, Y.Y. Aw, S.A. Sazali, W.M.A. Wan Ibrahim, *Mechanical Properties and Thermal and Electrical Conductivity of 3D Printed ABS-Copper Ferrite Composites via 3D Printing Technique*, Journal of Thermoplastic Composite Materials, 35(1), 3 (2019); https://doi.org/10.1177/0892705719869405.

[10] J. C. Hoh, I. I. Yaacob, *Polymer Matrix Templated Synthesis: Cobalt Ferrite Nanoparticles Preparation*, Journal of Materials Research, 17(12), 3105 (2002); https://doi.org/10.1557/jmr.2002.0449.

[11] J. Mazurenko, L. Kaykan, K. Bandura, O. Vyshnevskyi, M. Moiseienko, M. Kuzyshyn, N. Ostapovych, *Analysis of the Structural, Morphological, and Elastic Properties of Nanosized $CuFe_2O_4$ Spinel Synthesized via Sol-Gel Self-Combustion Method*, Physics and Chemistry of Solid State, 25(2), 380 (2024); https://doi.org/10.15330/pcss.25.2.380-390.

[12] M. Salavati-Niasari, T. Mahmoudi, M. Sabet, S. M. Hosseinpour-Mashkani, F. Soofivand, F. Tavakoli, *Synthesis and Characterization of Copper Ferrite Nanocrystals via Coprecipitation*, Journal of Cluster Science, 23(4), 1003 (2012); https://doi.org/10.1007/s10876-012-0486-7.

[13] U. Naresh, R. J. Kumar, K. C. B. Naidu, *Hydrothermal Synthesis of Barium Copper Ferrite Nanoparticles: Nanofiber Formation, Optical, and Magnetic Properties*, Materials Chemistry and Physics, 236, 121807 (2019); https://doi.org/10.1016/j.matchemphys.2019.121807.

[14] T. Kongkaew, K. Sakurai, *Low-Temperature Synthesis of Cubic Phase CuFe2O4 Powder*, Chemistry Letters, 46(10), 1493 (2017); https://doi.org/10.1246/cl.170632.

[15] J. Mazurenko, L. Kaykan, A. K. Sijo, M. Moiseienko, M. Kuzyshyn, N. Ostapovych, M. Moklyak, *The Influence of Reaction Medium pH on the Structure, Optical, and Mechanical Properties of Nanosized Cu-Fe Ferrite Synthesized by the Sol-Gel Autocombustion Method*, Journal of Nano Research, 81, 65 (2023); https://doi.org/10.4028/p-d2fqah.

[16] A. Lagashetty, K. Devendra, M. Sandhyarani, J. Rajeshwari, G. Galeppa, K. H. Lakshmidevi, B. B. Hajara, V. Veena, R. K. Preeti, S. K. Ganiger, *Microwave-Assisted Synthesis and Characterizations of Nanosized Copper Ferrite and Barium Titanate for Antimicrobial Applications*, Current Chemistry Letters, 13(2), 425 (2024); https://doi.org/10.5267/j.ccl.2023.10.003.

[17] N. Hamdi, W. Belam, *Structural, Electrical and Magnetic Properties of Copper-Substituted Co0.8-xNi0.2 Ferrites Synthesized by Sol–Gel Autocombustion Process*, Journal of Electronic Materials, 52(9), 5996 (2023); https://doi.org/10.1007/s11664-023-10519-2.

[18] J. Mazurenko, L. Kaykan, J. M. Michalik, M. Sikora, E. Szostak, O. Vyshnevskyi, K. Bandura, L. Turovska, *Enhanced Synthesis of Copper Ferrite Magnetic Nanoparticles via Polymer-Assisted Sol-Gel Autocombustion Method for Magnetic Hyperthermia Applications*, Journal of Nano Research, 84, 95 (2024); https://doi.org/10.4028/p-JbV1lE

[19] L. S. Kaykan, J.S. Kaykan, I.P. Yaremiy, O.M. Ugorchuk, B.Y. Deputat, M.O. Nykoliuk, *Synthesis, Structure and Dielectric Properties of Magnesium-Substituted Lithium Ferrite*, Journal of Nano- and Electronic Physics, 8(4(2)), 04066-1 (2016); https://doi.org/10.21272/jnep.8(4(2)).04066.

[20] Q.G. Jia, S.H. Liang, Q.X. Wang, *Preparation and Performance of CuFe2O4 and ZnFe2O4 Magnetic Nanocrystals*, Materials Research Express, 8(12), 125012 (2021); https://doi.org/10.1088/2053-1591/ac40b6.

[21] S. Gaffar, A. Kumar, J. Alam, U. Riaz, *Efficient Visible Light–Induced Photocatalytic Degradation of Tetracycline Hydrochloride Using CuFe2O4 and PANI/CuFe2O4 Nanohybrids*, Environmental Science and Pollution Research International, 30(50), 108878 (2023); https://doi.org/10.1007/s11356-023-29976-7.

[22] J. Li, S. Liu, X. Xie, J. Huang, S. Wang, H. Fang, *UV–Vis Photodetector Based on Electrospun MgFe2O4 Microfibers*, Materials Letters, 370, 136886 (2024); https://doi.org/10.1016/j.matlet.2024.136886.

[23] M. Zulqarnain, S.S. Ali, C.H. Wan, U. Hira, A. Hussain, G. Farid, *Structural Modifications, Low Temperature Magnetic Behavior and Optoelectronic Trends in A-Site Substituted Spinel Ferrites*, Materials Science & Engineering. B, Solid-State Materials for Advanced Technology, 298, 116829 (2023); https://doi.org/10.1016/j.mseb.2023.116829.

[24] R.S. Shitole, V.K. Barote, S.B. Kadam, R.H. Kadam, *Williamson-Hall Strain Analysis, Cation Distribution and Magnetic Interactions in Dy3+ Substituted Zinc-Chromium Ferrite*, Journal of Magnetism and Magnetic Materials, 588, 171468 (2023); https://doi.org/10.1016/j.jmmm.2023.171468.

[25] J. Mazurenko, L. Kaykan, A. Zywczak, V. Kotsyubynsky, K. Bandura, M. Moiseienko, A. Vytvytskyi, *Study of Li-Al Ferrites by Nuclear Magnetic Resonance, UV-Spectroscopy, and Mossbauer Spectroscopy*, Journal of Nano- and Electronic Physics, 15(2), 02020 (2023); https://doi.org/10.21272/jnep.15(2).02020.

[26] P. Kumar, M.C. Mathpal, R. Dhyani, R.C. Srivastava, M.A. G. Soler, J. Maze, H. C. Swart, *Optical Behavior of Ferrite Nanoparticles and Thin Films, in Ferrite Nanostructured Magnetic Materials*, Elsevier, 557 (2023).

[27] B.K. Ostafiychuk, L.S. Kaykan, J.S. Mazurenko, B.Y. Deputat, S.V. Koren, *Effect of Substitution on the Mechanism of Conductivity of Ultra Dispersed Lithium-Iron Spinel, Substituted with Magnesium Ions*, Journal of Nano- and Electronic Physics, 9(5), 05018-1 (2017); https://doi.org/10.21272/jnep.9(5).05018.

[28] E.E. Ateia, A.T. Mohamed, *Correlation Between the Physical Properties and the Novel Applications of Mg0.7Cu0.3Fe2O4 Nano-Ferrites*, Journal of Materials Science: Materials in Electronics, 28(14), 10035 (2017); https://doi.org/10.1007/s10854-017-6762-4.

[29] I. Khan, K. Saeed, I. Zekker, B. Zhang, A. H. Hendi, A. Ahmad, S. Ahmad, N. Zada, H. Ahmad, L. A. Shah, T. Shah, I. Khan, *Review on Methylene Blue: Its Properties, Uses, Toxicity and Photodegradation*, Water, 14(2), 242 (2022); https://doi.org/10.3390/w14020242.

[30] S. Sonia, H. Kumari, S. Chahal, S. Devi, S. Kumar, S. Kumar, P. Kumar, A. Kumar, *Spinel Ferrites/Metal Oxide Nanocomposites for Waste Water Treatment*, Applied Physics. A, Materials Science & Processing, 129(2) (2023); https://doi.org/10.1007/s00339-022-06288-0.

[31] M.V. Gerbaldo, S.G. Marchetti, S.M. Mendoza, V.R. Elias, S.N. Mendieta, M.E. Crivello, *Photocatalytic Degradation of Sodium Diclofenac Using Spinel Ferrites: Kinetic Aspects*, Topics in Catalysis, 65(13–16), 1419 (2022); https://doi.org/10.1007/s11244-022-01627-0.

[32] M. Sundararajan, V. Sailaja, L. John Kennedy, J. Judith Vijaya, *Photocatalytic Degradation of Rhodamine B Under Visible Light Using Nanostructured Zinc Doped Cobalt Ferrite: Kinetics and Mechanism*, Ceramics International, 43(1), 540 (2017); https://doi.org/10.1016/j.ceramint.2016.09.191.

[33] A. Nawaz, A. Khan, N. Ali, P. Mao, X. Gao, N. Ali, M. Bilal, H. Khan, *Synthesis of Ternary-Based Visible Light Nano-Photocatalyst for Decontamination of Organic Dyes-Loaded Wastewater*, Chemosphere, 289(133121), 133121 (2022); https://doi.org/10.1016/j.chemosphere.2021.133121.

[34] U. Manhas, I. Qadir, A. K. Atri, S. Sharma, S. Singh, M. Sharma, P. Sharma, D. Singh, *Effect of Sintering Temperature on Magnetic, Catalytic and Photocatalytic Properties of Cu-Co-Mn Ferrite Catalyst*, Ceramics International (2024); https://doi.org/10.1016/j.ceramint.2024.09.028.

[35] S. Patar, R. Mittal, A. Dutta, B. K. Bhuyan, L. J. Borthakur, *Algae Derived N-Doped Mesoporous Carbon Nanoflakes Fabricated with Nickel Ferrite for Photocatalytic Removal of Congo Red and Rhodamine B Dyes*, Surfaces and Interfaces, 51(104710), 104710 (2024); https://doi.org/10.1016/j.surfin.2024.104710.

[36] T. Tatarchuk, A. Shyichuk, M. Naushad, N. Danyliuk, I. Lapchuk, *Copper-Substituted Magnetite as a Fenton-Like Catalyst Boosted with Electromagnetic Heating*, Journal of Water Process Engineering, 60(105170), 105170 (2024); https://doi.org/10.1016/j.jwpe.2024.105170.

Ю. Мазуренко[1,2], Л. Кайкан[3], В. Мокляк[3,4], М. Петришин[5], О. Мазуренко[5], С. Лелеко[1]

Фотокаталітична деградація метиленового синього у водному середовищі з використанням заміщеного магнієм мідного фериту як магнітного каталізатора

[1]*Івано-Франківський національний медичний університет, м. Івано-Франківськ, Україна, yumazurenko@ifnmu.edu.ua;*
[2]*Факультет фізики та прикладних комп'ютерних наук, університет AGH у Кракові, Краків, Польща;*
[3]*Інститут металофізики ім. Г. В. Курдюмова НАН України, Київ, Україна, larysa.kaykan@gmail.com;*
[4]*Івано-Франківський національний технічний університет нафти і газу, Івано-Франківськ, Україна, volodymyr.mokliak@nung.edu.ua;*
[5]*Прикарпатський національний університет імені Василя Стефаника, Івано-Франківськ, Україна, m.l.petryshyn@pnu.edu.ua*

Нанорозмірний ферит міді, заміщений іонами магнію був синтезований за допомогою методу золь-гель автоспалювання, використовуючи поліетиленгліколь (M_W=2000) як паливо та хелатуючий агент. Структурні властивості досліджувалися методами X-променевої дифракції (XRD). Дані дослідження підтвердили утворення кубічної шпінельної структури з просторовою групою Fd3m для всіх зразків. Оптичні дослідження показали, що ширина забороненої зони збільшується від 1,51 еВ для $CuFe_2O_4$ до 1,62 еВ для $MgFe_2O_4$, що вказує на зміни в електронній структурі внаслідок заміщення магнієм. Фотокаталітичні дослідження показали, що чистий $CuFe_2O_4$ найефективніше розкладає барвник метиленовий синій, забезпечуючи майже повну деградацію барвника за 160 хвилин. Зразки із заміщенням магнієм (x = 0.4 і x = 0.6) також продемонстрували значну фотокаталітичну активність, хоч і зі зниженою швидкістю порівняно з чистим $CuFe_2O_4$. Оцінка фотокаталітичної ефективності проводилася за допомогою різних кінетичних моделей, включаючи кінетику першого і другого порядку, модель Ленгмюра-Хіншельвуда та двопараметричний розподіл Вейбула.

Ключові слова: Наноферит міді; Фотокаталітична деградація; Метиленовий синій; Кінетичне моделювання; Модель Ленгмюра-Хіншельвуда; Модель розподілу Вейбула.